Development 137, 2587-2596 (2010) doi:10.1242/dev.043745

A model of Costeff Syndrome reveals metabolic and protective functions of mitochondrial OPA3

Wuhong Pei[1], Lisa E. Kratz[2], Isa Bernardini[1], Raman Sood[3], Tohei Yokogawa[4], Heidi Dorward[1], Carla Ciccone[1], Richard I. Kelley[2], Yair Anikster[5], Harold A. Burgess[4], Marjan Huizing[1] and Benjamin Feldman[1,*]

SUMMARY

Costeff Syndrome, which is caused by mutations in the *OPTIC ATROPHY 3* (*OPA3*) gene, is an early-onset syndrome characterized by urinary excretion of 3-methylglutaconic acid (MGC), optic atrophy and movement disorders, including ataxia and extrapyramidal dysfunction. The OPA3 protein is enriched in the inner mitochondrial membrane and has mitochondrial targeting signals, but a requirement for mitochondrial localization has not been demonstrated. We find zebrafish *opa3* mRNA to be expressed in the optic nerve and retinal layers, the counterparts of which in humans have high mitochondrial activity. Transcripts of zebrafish *opa3* are also expressed in the embryonic brain, inner ear, heart, liver, intestine and swim bladder. We isolated a zebrafish *opa3* null allele for which homozygous mutants display increased MGC levels, optic nerve deficits, ataxia and an extrapyramidal movement disorder. This correspondence of metabolic, ophthalmologic and movement abnormalities between humans and zebrafish demonstrates a phylogenetic conservation of OPA3 function. We also find that delivery of exogenous Opa3 can reduce increased MGC levels in *opa3* mutants, and this reduction requires the mitochondrial localization signals of Opa3. By manipulating MGC precursor availability, we infer that elevated MGC in *opa3* mutants derives from extra-mitochondrial HMG-CoA through a non-canonical pathway. The *opa3* mutants have normal mitochondrial oxidative phosphorylation profiles, but are nonetheless sensitive to inhibitors of the electron transport chain, which supports clinical recommendations that individuals with Costeff Syndrome avoid mitochondria-damaging agents. In summary, this paper introduces a faithful Costeff Syndrome model and demonstrates a requirement for mitochondrial OPA3 to limit HMG-CoA-derived MGC and protect the electron transport chain against inhibitory compounds.

KEY WORDS: Zebrafish, OPA3, Costeff Syndrome, 3-Methylglutaconic aciduria, Mitochondria, Metabolic disorder

INTRODUCTION

Costeff Syndrome (OMIM 258501), also called Type III 3-Methylglutaconic aciduria (Type III MGA) or Optic Atrophy 3 disorder, is caused by mutations in the *OPA3* gene (Anikster et al., 2001). In addition to MGA, individuals with Costeff Syndrome display optic atrophy and extrapyramidal movement disorders and more variably develop ataxia, spasticity, hyperreflexia, cognitive deficits and/or a loss of visual acuity (Costeff et al., 1989).

Costeff Syndrome is a rare autosomal recessive disorder with fewer than 50 documented cases worldwide. OPA3 is a 179 amino acid protein with mitochondrial leader and targeting signals at the N terminus, but no other recognizable structural motifs (Fig. 1A). Three Costeff Syndrome-causing *OPA3* mutations have been identified: 40 patients of Iraqi-Jewish origin homozygous for a splice junction mutation (Fig. 1A; IVS-1); one patient of Kurdish-Turkish origin homozygous for an in-frame deletion of six conserved amino acids (Fig. 1A; Del.); and one patient of Indian origin homozygous for a nonsense mutation (Fig. 1A; Q139X) (Anikster et al., 2001; Ho et al., 2008; Kleta et al., 2002). In addition to *OPA3* mutations causing Costeff Syndrome, two *OPA3* missense mutations, G93S and Q105E, in heterozygous state have been associated with a distinct and somewhat milder dominant disorder termed Autosomal Dominant Optic Atrophy and Cataract (ADOAC; OMIM 165300) in 14 patients in France (Ferre et al., 2009; Reynier et al., 2004).

Costeff Syndrome is one of five MGA syndromes that share a common signature of markedly increased urinary levels of the organic acid 3-methylglutaconic acid (MGC) (Gibson et al., 1993; Gunay-Aygun, 2005). MGC exists in equilibrium with 3-methylglutaric acid (MGR), which also is increased in Costeff Syndrome patients. As a result, MGC measurements can serve as a proxy for both MGC and MGR. Although the best documented origin of MGC in human metabolism is from mitochondrial 3-methylglutaconyl-CoA, Edmond and Popjak (Edmond and Popjak, 1974) and Schroepfer (Schroepfer, 1981) proposed and/or showed evidence for several extra-mitochondrial sources of MGC, all of which derive ultimately from 3-hydroxy-3-methylglutaryl-coenzyme A (HMG-CoA; Fig. 1B) (Landau and Brunengraber, 1985; Poston, 1976).

Although the cellular function of OPA3 is unknown, several lines of evidence suggest a role in the inner mitochondrial membrane (IMM), where the electron transport chain complexes and multiple metabolite and protein import systems are located (Fig. 1B). First, human OPA3 has functional mitochondrial leader and targeting signals, and proteomic analysis has found murine

[1]Medical Genetics Branch, National Human Genome Research Institute, Bethesda, MD 20892, USA. [2]Kennedy Krieger Institute, Johns Hopkins University, Baltimore, MD 21205, USA. [3]Zebrafish Core Facility, National Human Genome Research Institute, Bethesda, MD 20892, USA. [4]Laboratory of Molecular Genetics, Eunice Kennedy Shriver National Institute of Child Health and Human Development, Bethesda, MD 20892, USA. [5]Metabolic Disease Unit, Safra Children's Hospital, Sheba Medical Centre, Sackler Medical School, Tel Aviv University, Tel-Hashomer 52621, Israel.

*Author for correspondence (bfeldman@mail.nih.gov)

Accepted 21 May 2010

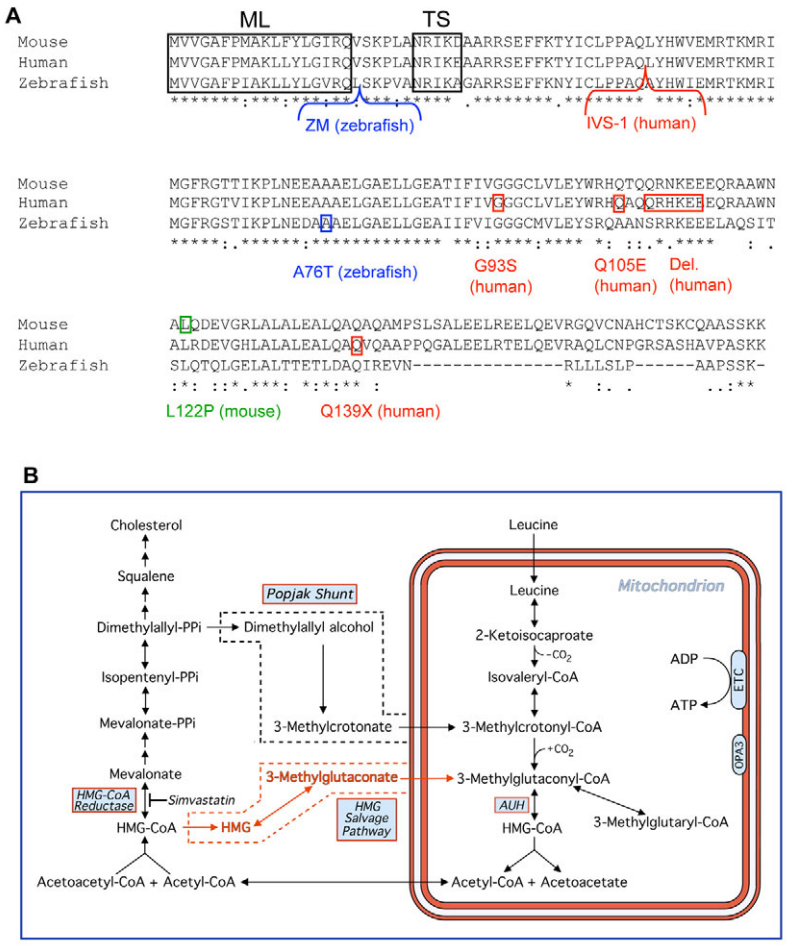

Fig. 1. OPA3 mutations and MGC-associated pathways. (**A**) Alignment of mouse, human and zebrafish OPA3. Consensus key: *, identical residues; :, strongly conserved residues; ., weakly conserved residues; –, no orthologous residues. Black boxes frame the mitochondrial leader (ML) and targeting sequences (TS). Small red, blue and green boxes indicate human (red), zebrafish (blue) and mouse (green) point mutations. Red and blue brackets show insertion sites of the human IVS-1 mutation (red) and zebrafish retroviral DNA (blue). (**B**) Biochemical sources of MGC. Enzymatic steps known to be reversible are indicated with double-headed arrows. Two arrows in sequence, as well as the double-headed arrow connecting mitochondrial and extra-mitochondrial acetyl-CoA, represent two or more enzymatic steps. The Popjak shunt was proposed as a mechanism to explain experimental data showing that a substantial amount of carbon from mevalonate ultimately is metabolized in mitochondria, but the specific steps and localization of the shunt are not proven. The elements of the non-canonical 'HMG salvage pathway' supported by the studies in this work are indicated in red.

Opa3 to be enriched in the IMM (Da Cruz et al., 2003; Huizing et al., 2010). Second, several other optic atrophy disorders and one form of MGA (Barth Syndrome/MGA II, OMIM 302060) are caused by mutations in proteins required for IMM functional integrity (Huizing et al., 2005). Third, a mouse model of Costeff Syndrome has mitochondrial defects (Davies et al., 2008). Based on this evidence, the current clinical recommendation is for individuals with Costeff Syndrome to avoid medications known to impair mitochondrial function or to increase oxidative stress (Gunay-Aygun et al., 2010).

OPA3 is highly conserved across many species, spanning from fungi to human. In this paper, we describe the embryonic expression of zebrafish *opa3* and explore the function of OPA3 by generating *opa3* mutants and challenging them in several ways. The zebrafish mutants recapitulate key Costeff Syndrome symptoms, including MGC aciduria, and we show that this excess MGC probably derives from extra-mitochondrial HMG-CoA. We further show that the reduction of MGC levels by Opa3 is dependent on its delivery to mitochondria. Finally, we show that *opa3* mutant embryos are sensitive to electron transport chain-inhibiting compounds.

MATERIALS AND METHODS

Zebrafish husbandry

Embryos were from natural crosses and staged conventionally (Kimmel et al., 1995). Except where otherwise indicated, $opa3^{ZM/ZM}$ and $opa3^{A76T/A76T}$ embryos and larvae came from respective homozygous parents and wild-type ($opa3^{+/+}$) controls were from the same genetic background. All microinjections were performed in one- to two-cell stage embryos. The antisense morpholinos (MO) sequences were as follows: standard MO, CCTCTTACCTCAGTTACAATTTATA; Auh MO, TCTACACCT-CACTATAGCCGCCATG; Auh mismatch MO, TCaAgACCTgA-CTATAcCCcCCATG (the lower cases indicate the five mismatched bases). 5 ng MOs were injected. mRNAs were synthesized using the mMessage mMachine SP6 Kit (Ambion). Whole-mount in situ hybridization (WISH) was standard (Thisse and Thisse, 1998). For WISH on embryos older than 24 hours, N-phenylthiourea (Sigma) was used to suppress pigment development.

Histology

WISH-stained 3-day-old embryos were embedded in JB-resin and sectioned at 7 μm. WISH-stained 5-day-old embryos, as well as larvae and adults, were embedded in paraffin and sectioned at 5 μm, then counterstained as indicated (HistoServ; Germantown, MD).

Mitochondrial targeting

MLTS-GFP fusion constructs were created by inserting the mitochondrial leader and targeting signals of *opa3* into pEGFP-N1 plasmids (Clontech), and transfected into human fibroblasts then cultured, counterstained with MitoTracker Deep Red 633 (Molecular Probes) and imaged as previously described (Huizing et al., 2010). Control transfections used the pmaxGFP plasmid. The same CMV promoter was used in both constructs.

MGC measurements

One-hundred zebrafish embryos per data point were homogenized in 1 ml PBS, and individual adult zebrafish were homogenized in 40 ml PBS. Organic acids were extracted from 1 ml aliquots using ethyl acetate. MGC was measured by isotope-dilution gas chromatography-mass spectroscopy (GC-MS) as previously described (Kelley and Kratz, 1995). Protein

concentrations were determined with a BCA protein assay kit (Pierce). Each panel represents parallel runs, except for Fig. 7C where the Ctrl MO versus Auh MO and *opa3*$^{+/+}$ versus *opa3*$^{ZM/ZM}$ were from different runs. Differences in measured MGC levels from different runs probably reflect variations in extraction efficiencies or column conditions.

Behavioral assays

Analysis of spontaneous forward scoots and turns was carried out as described (Burgess and Granato, 2007). Briefly, high speed video recordings (1000 fps) of 30 s duration were taken of larvae using a DRS Lightning high-speed camera (Del Imaging Systems, Cheshire, CT). The testing arena was lit from above at 650 μW/cm^2 with a white LED, with an infrared array positioned below the stage providing illumination for recording. Larvae were tested in four groups of 25 at 5, 6 and 7 days. Video recordings were analyzed with the Flote software package. All statistical analysis of larval behavior was performed using SPSS.

For buoyancy measurements, up to 15 adult fish were anesthetized in 240 ml of system water supplemented with 0.025% Tricaine (w/v), transferred to a 250 ml graduated cylinder and their positions (top or bottom) recorded. Fish were promptly allowed to recover in clean system water.

To measure maximum angles of ascent and descent and heights in tanks, adult fish were pre-adjusted to 250 μW/cm^2 lighting for 1.5 hours, then individually transferred to a 1 l tank, pre-adjusted for 5 minutes then filmed for 5 minutes at five frames per second using a microEye IDS-1545LEM camera (1stVision, Andover, MA) and analysis was done with Image J software. Heights were calculated as the average of all 1500 frames. Maximum angles of ascent and descent represent summed averages from the five frames showing the largest angle of ascent and the five frames showing the largest angle of descent.

Leucine supplementation and endogenous leucine measurement

300 mg of leucine (Sigma) was dissolved in 5 ml 1 N HCl and the pH was adjusted to 7 with 2 N NaOH. A 12 mg/ml solution of leucine in embryo medium [0.006% red sea salts (w/v) and 0.0001% methylene blue (w/v), pH~6.4] was injected into embryos (~1.5 nl per embryo) at the one- to 2-cell stage. Embryos were further incubated in a 2 mg/ml solution of leucine in embryo medium. For embryonic leucine measurements, 50 embryos per data point were collected in 100 μl embryo medium and homogenized. The lysate was deproteinated by mixing with 80 μl Li Citrate buffer (pH 2.2) and 20 μl 33% sulpho-salicylic acid, cleared through a 3KMWCO Viva-spin ultra-filter and measured on a Biochrom 30 amino acid analyzer.

Oxygen flux measurements

Four 14-somite stage embryos in their chorions were placed in each assayed well of an XF24 islet capture plate in 500 μl filtered (0.22 μm) medium (0.006% sea salt), covered with rings (mesh side up) and loaded into a Seahorse XF24 analyzer set at 30°C. The rate of oxygen flux was measured before and after the addition of 75 μl each of the following compounds: oligomycin (700 μg/ml), FCCP (15 μM) and antimycin A (60 μg/ml).

ATP production assay

Fifteen 30-hour-old embryos per data point, either untreated or antimycin A treated, were harvested and extracted for ATP as previously described (Yang et al., 2002). ATP concentrations were immediately measured using the Enliten ATP Assay Kit (Promega). The ATP production in untreated *opa3*$^{+/+}$ controls was defined as 100% and used to normalize the ATP concentrations in other samples.

Drug treatments

For measuring drug sensitivity, fifty four-cell stage embryos were incubated in a 100 mm×20 mm glass dish containing 30 ml embryo medium, with or without supplementation of 20 nM rotenone, 1 ng/ml antimycin A, 30 μM potassium cyanide (KCN), 0.2 μg/ml oligomycin, 80 nM staurosporine or 0.5 μM simvastatin (all from Sigma). Phenotypes were scored and photographed at 1 day. For *opa3*$^{ZM/+}$ incrosses, individual embryos were genotyped after scoring. For MGC measurements after simvastatin treatment, 100 embryos per dish were treated as above and collected at 1 day for MGC measurements.

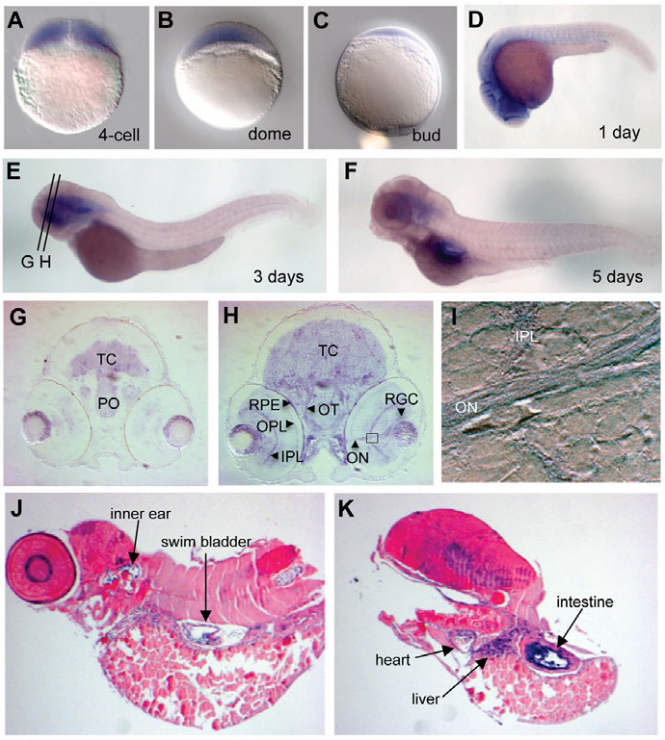

Fig. 2. Zebrafish *opa3* expression in the brain, eye and other organs during embryogenesis. (**A-F**) Whole-mount in situ stains of *opa3* mRNA. Embryonic stages are as labeled. Orientations: A-F,J-K, lateral views; G-I, frontal views. (**G-I**) *opa3* expression in brain and eyes. (G,H) Transverse sections (approximate positions shown in E) through a 3-day-old *opa3*-stained embryo. TC, tectum; PO, pre-optic region; RPE, retinal pigment epithelium; OPL, outer plexiform layer; IPL, inner plexiform layer; OT, optic tract; ON, optic nerve; RGC, retinal ganglion cells. I shows a higher magnification view of the boxed region in H. (**J**,**K**) *opa3* mRNA expression in a 5-day-old embryo. Embryos were laterally sectioned and counterstained with nuclear Fast Red.

RESULTS

Enrichment of *opa3* in the embryonic nervous system and internal organs

Human *OPA3* is expressed ubiquitously in adults, but symptoms of Costeff Syndrome suggest particular requirements in the nervous system (Anikster et al., 2001). To determine when and where Opa3 might act during zebrafish development, we localized *opa3* transcripts by whole-mount in situ hybridization (WISH). *opa3* is expressed in 4-cell stage embryos (Fig. 2A), prior to the onset of zygotic transcription, indicating that the mRNA is present in oocytes. Transcripts of *opa3* are ubiquitously distributed through the tailbud stage of development (Fig. 2B,C) then become progressively enriched in the brain (Fig. 2D). This enrichment persists through 5 days of development, when enriched *opa3* expression also becomes apparent in internal organs (Fig. 2E,F). Sections of *opa3*-stained 3-day-old embryos reveal concentrations in the tectum, preoptic region, optic tract, optic nerve and other regions of the retina, namely retinal ganglion cells, inner and outer plexiform layers and retinal pigment epithelium (Fig. 2G-H). Higher magnification views of *opa3*-labeled optic nerves show that *opa3* mRNA is localized in the axons of the optic nerve (Fig. 2I). Sections of *opa3*-stained 5-day-old embryos also reveal transcripts in the inner ear, swim bladder, heart, liver and intestinal epithelium (Fig. 2J-K).

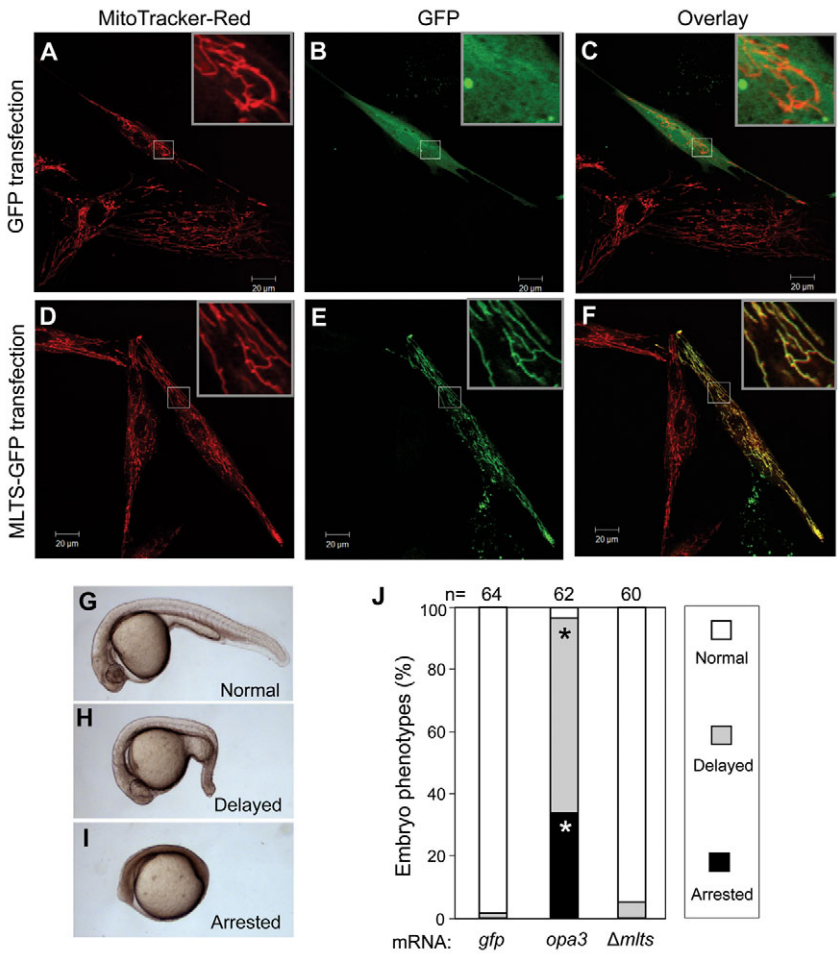

Fig. 3. Zebrafish Opa3 has functional mitochondrial leader and targeting sequences (MLTS). (**A-F**) Targeting assay. Human fibroblasts were transfected with plasmids expressing GFP or GFP linked to the MLTS of Opa3 (MLTS-GFP; Opa3 residues A1-S34 fused to the N terminus of GFP). A and D show the MitoTracker Red stains alone; B and E show GFP fluorescence; and C and F show the overlap of both signals. An enlarged inset in each image allows better visualization. (**G-I**) Gain-of-function assay. Wild-type embryos were injected with 200 pg of *opa3* mRNA or mutated *opa3* mRNA (*Δmlts*) from an *opa3* vector in which the MLTS was deleted in frame (residues M1-K28 deleted, A29 converted to M). Embryonic phenotypes were scored at day 1. (**J**) Incidence of overexpression phenotypes. The number of embryos scored for each mRNA injection is indicated. Asterisks (*) indicate statistically significant increases (chi-square test, $P<10^{-6}$) between the *opa3* mRNA injected embryos and *Δmlts* mRNA-injected embryos. No difference was seen between *Δmlts* mRNA-injected embryos and *gfp* mRNA-injected embryos ($P=0.2789$).

Conserved mitochondrial localization of OPA3

We recently showed that human OPA3-GFP fusion proteins are targeted to mitochondria in human fibroblast cells (Huizing et al. 2010). There are four amino acid differences between the human OPA3 mitochondrial leader and targeting sequences (MLTS), and the analogous portion of zebrafish Opa3 (Fig. 1A). The putative zebrafish MLTS is not recognized as a mitochondrial signal by prediction software (http://psort.nibb.ac.jp/); however, we find that it successfully targets GFP to human fibroblast cell mitochondria (Fig. 3A-F). We also observe that microinjection of 200 pg *opa3* mRNA into zebrafish embryos causes developmental arrest and delays in an MLTS-dependent manner (Fig. 3G-J). Thus, the MLTS of zebrafish Opa3 is sufficient for protein localization to mitochondria and is necessary for the gain-of-function effects of Opa3 in embryos.

Generation of *opa3* mutants

To determine the developmental requirements for Opa3, we obtained two mutant *opa3* alleles. The ZM_00365842 ($opa3^{ZM}$) allele has a 5.2 kb retroviral DNA insertion just downstream of mitochondrial leader signal of *opa3* (Fig. 1A). This allele was identified by sequencing insertion sites in a library of retrovirally mutagenized sperm (Jao et al., 2008). The line was then derived by in vitro fertilization (performed by Znomics) and we verified the disruption by sequencing the viral-host DNA junctions (data not shown) and by RT-PCR analysis (see Fig. S1 in the supplementary material). The predicted $opa3^{ZM}$ product comprises the first 19 amino acids, followed by five virally encoded amino acids and a virally encoded termination codon. Our RT-PCR analysis indicates that erroneous splicing of the $opa3^{ZM}$ allele causes inclusion of at least 60 nucleotides from intron 1, which introduces additional termination codons in all three frames (see Fig. S1 in the supplementary material). A second mutant allele ($opa3^{A76T}$) was derived by TILLING and carries a guanosine 226 to adenosine substitution, converting a conserved alanine (residue 76) to threonine (Fig. 1A; see Fig. S1A in the supplementary material) (Sood et al., 2006).

Recapitulation of MGC aciduria in *opa3* mutants

To determine whether Opa3 deficiency leads to increased levels of MGC in zebrafish, we compared MGC levels in $opa3^{+/+}$, $opa3^{ZM/ZM}$ and $opa3^{A76T/A76T}$ embryos using isotope-dilution gas chromatography-mass spectroscopy (GC-MS). A substantial increase in the level of MGC was detected in 5-day-old mutant embryos and a more moderate increase was found in mutant adult fish (Fig. 4A). The magnitude of these increases is comparable with that seen in Costeff Syndrome (Elpeleg et al., 1994). No MGC increase was seen in heterozygous 5-day-old embryos (Fig. 4A). Therefore, as in Costeff Syndrome, increased MGC is a recessive phenotype. Although we observed comparable elevations of MGC in $opa3^{ZM/ZM}$ and $opa3^{A76T/A76T}$ mutants, we consider the $opa3^{A76T}$ allele to be a hypomorph, because it fails to produce other phenotypic features we observe in $opa3^{ZM/ZM}$ mutants. Confirming that the MGC increase is specific to Opa3 deficiency, injection of 25 pg *opa3* mRNA suppressed the MGC increase in $opa3^{ZM/ZM}$ embryos (Fig. 4B).

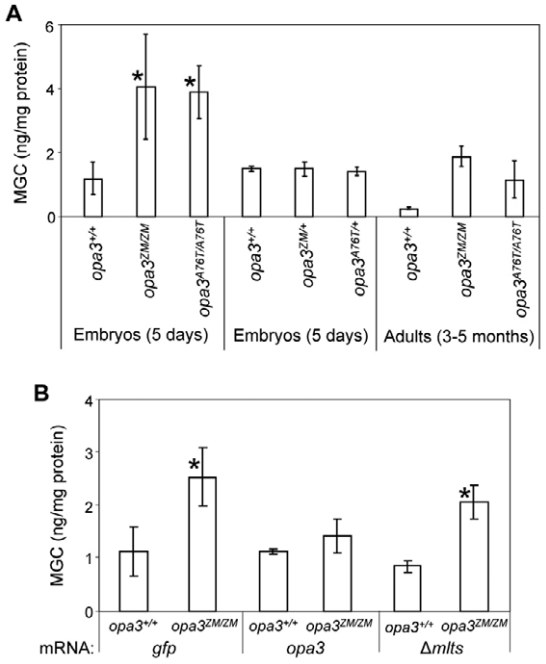

Fig. 4. MGC elevation in *opa3* mutants and its MLTS-dependent reduction by Opa3. MGC values are normalized to protein yields of extracts. (**A**) Elevated MGC in embryonic and adult homozygotes. (**B**) Rescue of increased MGC with *opa3* mRNA, but not Δmlts mRNA. *opa3*$^{+/+}$ and *opa3*$^{ZM/ZM}$ embryos were injected with 25 pg of either *opa3* mRNA, *Δmlts opa3* mRNA or control *gfp* mRNA, and harvested the next day to measure MGC levels. Injected mRNAs are as indicated. Asterisks (*) indicate statistically significant increases (*t*-test, $P<0.05$). MGC increases were also seen in adult mutants, but the significance was not quantified because only two measurements were available.

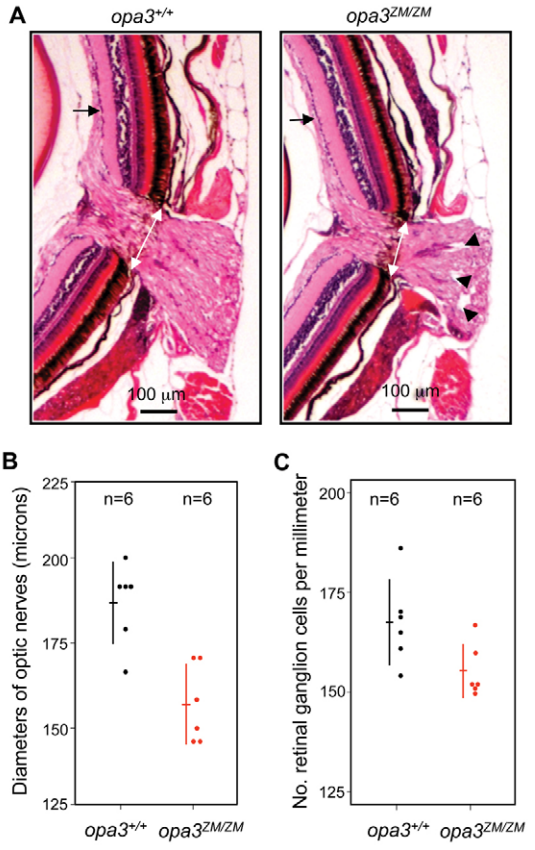

Fig. 5. Optic nerve deficits in *opa3*$^{ZM/ZM}$ mutants. (**A**) Sections of *opa3*$^{+/+}$ and *opa3*$^{ZM/ZM}$ adult retinas. Three 1-year-old adult fish for each genotype were coronally sectioned and Hematoxylin and Eosin stained. One representative section is shown for each genotype. White arrows indicate optic nerve diameters and measurement points. Arrowheads indicate optic nerve lesions. Black arrows indicate retinal ganglion cells. (**B**,**C**) Comparison of optic nerve diameters (B) and retinal ganglion cell numbers (C) in *opa3*$^{+/+}$ and *opa3*$^{ZM/ZM}$ adult fish. Each dot represents a single measurement, horizontal lines show the average and vertical lines show the standard deviation. Red lines and data points are significantly different from black lines and data points (*t*-test, $P<0.015$).

Our ability to suppress the MGC increase with exogenous *opa3* mRNA allowed us to test the functional requirement for Opa3 localization to mitochondria. We found that *opa3* mRNA lacking the MLTS (*Δmlts*) is unable to suppress the MGC increase in *opa3*$^{ZM/ZM}$ mutants (Fig. 4B). Therefore, the effect of Opa3 on MGC levels depends on its localization to mitochondria.

Optic nerve deficits in *opa3* mutants

Individuals with Costeff Syndrome display optic nerve pallor and retinal thinning from an early age. No overt morphological phenotypes were observed in *opa3*$^{ZM/ZM}$ or *opa3*$^{A76T/A76T}$ embryos or adults (see Fig. S2A-C in the supplementary material and data not shown), and the optic nerves and other tissues of 6-day-old *opa3*$^{ZM/ZM}$ larvae appeared normal in histological sections (see Fig. S2D-E in the supplementary material). However, sections of 1-year-old *opa3*$^{ZM/ZM}$ adults revealed a significant reduction in optic nerve diameters (Fig. 5A, white arrows; Fig. 5B). We also observed lesions in 4 out of 6 *opa3*$^{ZM/ZM}$ optic nerves (Fig. 5A, arrowheads), with comparable lesions in only one out of 12 optic nerves from other genotypes. We further noted a moderate decrease in the number of retinal ganglion cell bodies, which are the source of the axons comprising the optic nerve (Fig. 5A, black arrows; Fig. 5C). This indicates that the reduced optic nerve diameter is at least partially due to a reduced number of contributing axons.

Ataxia, loss of buoyancy control and hypokinesia in *opa3* mutants

Although *opa3*$^{ZM/ZM}$ mutants are overtly indistinguishable from *opa3*$^{+/+}$ embryos, we noted a small fraction (12 out of 225) with dramatic alterations in swimming behavior. These affected fish position themselves vertically and swim towards the bottom of the tank, rising back towards the top of the tank between efforts (Fig. 6A; see Movie 1 in the supplementary material). This behavior has a variable age of onset, ranging from two to five months. Within 4 weeks of onset, the fish begin to linger close to the water's surface, often upside down. These fish become progressively emaciated and generally perish within 3 months of onset of the behavior.

Based on the intense up-and-down movements of affected fish, we hypothesized that Opa3 has a role in buoyancy control. We compared the neutral buoyancy of *opa3*$^{ZM/ZM}$ and control fish after rendering them unconscious with anesthesia. Whereas all control fish sink to the bottom of a test water column, more than 15% of *opa3*$^{ZM/ZM}$ fish float to the top (Fig. 6B), including mutants with

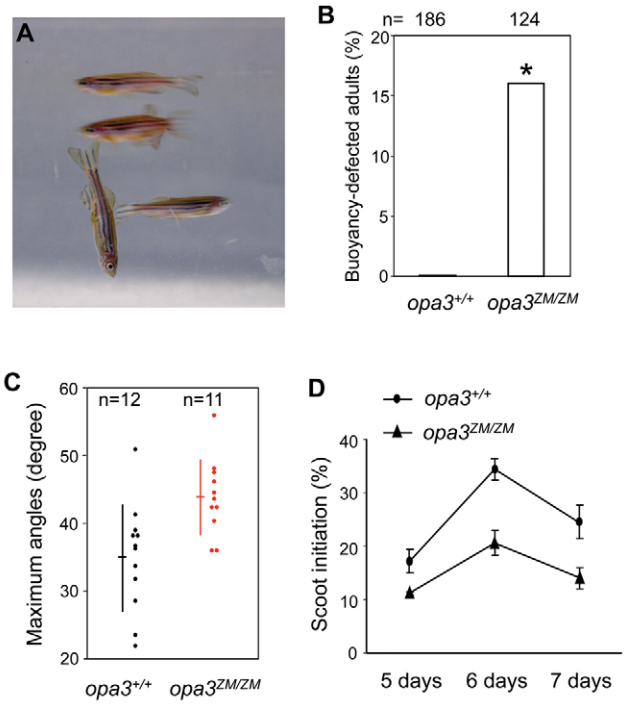

Fig. 6. Behavioral anomalies of *opa3*$^{ZM/ZM}$ mutants. (**A**) Image of one abnormally swimming *opa3*$^{ZM/ZM}$ adult fish and three normal *opa3*$^{ZM/ZM}$ siblings. (**B**) Increased buoyancy in *opa3*$^{ZM/ZM}$ adult fish. Asterisk (*) indicates the statistical significance of the increase (chi-square test, *P*=2.1e–7). (**C**) Exaggerated vertical turns by *opa3*$^{ZM/ZM}$ adult fish. Each dot represents combined average of maximum ascent and descent angles observed for an individual fish. Horizontal lines show the overall average and vertical lines show the standard deviations. Red lines and data points are significantly different from black lines and data points (*t*-test, *P*=0.0055). (**D**) Reduced spontaneous scoot initiation by *opa3*$^{ZM/ZM}$ larvae. Circles show the average scoot frequency for four groups of 25 *opa3*$^{+/+}$ larvae and triangles show the average scoot frequency for four groups of 25 *opa3*$^{ZM/ZM}$ larvae, each measured on three consecutive days. A significant reduction was observed in *opa3*$^{ZM/ZM}$ larvae (ANOVA test, F[1,9]=23.4, *P*=0.001).

apparently normal swimming behavior. In a search for more subtle alterations to swimming behavior, we selected adult control (*opa3*$^{+/+}$) and *opa3*$^{ZM/ZM}$ mutants with apparently normal swimming behaviors and documented their average positions in individual tanks as well as their maximum angles of ascent and descent. This revealed that maximum angles of ascent and descent are substantially larger among *opa3*$^{ZM/ZM}$ mutants (Fig. 6C). No difference was seen in the average tank position.

In light of the grossly impaired swimming in a subset of mutants, we consider the increased angles of ascent and descent across the population of *opa3*$^{ZM/ZM}$ fish to reflect a ‘subclinical’ defect in movement or balance control. This may be analogous to the ataxia (uncoordinated movements) seen in a subset of individuals with Costeff Syndrome (Costeff et al., 1989). Although ataxia can be associated with defects in the cerebellum, standard and TUNEL-stained histological sections through an adult *opa3*$^{ZM/ZM}$ fish revealed no obvious morphological abnormalities or increase in cell death in the cerebellum or other systems whose disruption might cause movement disorders, namely the inner ear (balance), the hypothalamus (autonomic control of balance and buoyancy), dorsal spinal cord neurons (motor control) or the swim bladder (buoyancy control) (see Fig. S3 in the supplementary material and data not shown).

A characteristic of Costeff Syndrome is the early onset of ophthalmologic and movement defects, so we assessed the vision and movements of zebrafish *opa3*$^{ZM/ZM}$ larvae. In addition to ataxia, individuals with Costeff Syndrome varyingly display reduced visual acuity, hyperreflexia, spastic movements and an extrapyramidal movement disorder such as chorea, a form of hyperkinesia, or bradykinesia (Costeff et al., 1989). Zebrafish larvae have a stereotypic set of behaviors with defined kinematic parameters, allowing us to undertake a number of behavioral assays. We identified an early-onset hypokinesia phenotype, reminiscent of the extrapyramidal movement defects seen in Costeff Syndrome. Wild-type zebrafish larvae normally initiate two types of movements: scoots and routine turns (Burgess and Granato, 2007). No significant change in the deployment of routine turns was detected. However *opa3*$^{ZM/ZM}$ larvae display a significant reduction in frequency of the initiation of scoot movements (Fig. 6D). Because reduced spontaneous movement initiation is analogous to human hypokinesia, which can result from reduced levels of tyrosine hydroxylase (a dopamine synthetic enzyme), we examined expression of tyrosine hydroxylase in *opa3*$^{ZM/ZM}$ embryos, but saw no meaningful difference from controls (see Fig. S4A in the supplementary material) (Wevers et al., 1999). We also asked whether an increase in the level of MGC can itself cause hypokinesia, but saw no changes in the scoot initiation of *opa3*$^{+/+}$ or *opa3*$^{ZM/ZM}$ embryos in whom endogenous MGC levels were increased by the addition of exogenous MGC (see Fig. S4B in the supplementary material). The other behavioral assays we ran indicated that *opa3*$^{ZM/ZM}$ larvae have normal visual function (see Fig. S2F-H in the supplementary material) and do not suffer from early onset ataxia, hyperreflexia or spasticity (see Fig. S4C-G in the supplementary material).

In summary, our behavioral examination of adult and larval *opa3*$^{ZM/ZM}$ mutants revealed a progressive loss of buoyancy control in a subset of fish, as well as more penetrant behaviors analogous to the ataxia and extrapyramidal disorders (bradykinesia) observed in Costeff Syndrome, but not the vision loss, hyperreflexia or spasticity.

Evidence for an HMG salvage pathway downstream of extra-mitochondrial HMG-CoA

Although various mitochondrial and extra-mitochondrial sources for MGC have been proposed and studied over the past three decades, the source of excess MGC in Costeff Syndrome and most other MGA Syndromes remains unclear. To clarify the origin of excess MGC in *opa3*$^{ZM/ZM}$ mutants, we performed two biochemical interventions: leucine supplementation and inhibition HMG-CoA reductase, as explained below.

The source of excess MGC is known for one MGA syndrome: Type I MGA (OMIM 250950). In Type I MGA, mitochondrial catabolism of leucine is disrupted by mutations in the AU RNA-binding protein/enoyl-Coenzyme A hydratase, and excess MGC is produced from the consequent build up of mitochondrial 3-methylglutaconyl-CoA (IJlst et al., 2002). Consistent with this, 3-hydroxyisovaleric acid, derived from 3-hydroxyisovaleryl-CoA (Fig. 1B), is also elevated in the urine of individuals with Type I MGA; interestingly, 3-hydroxyisovaleric acid is not increased in Costeff Syndrome (Type III MGA) or other MGAs, suggesting that a leucine-independent mechanism underlies MGC elevation in these diseases (Gibson et al., 1993). To test the hypothesis that Opa3 acts outside of the leucine catabolic pathway, we compared the efficiency of leucine catabolism in *opa3*$^{ZM/ZM}$ mutants and a

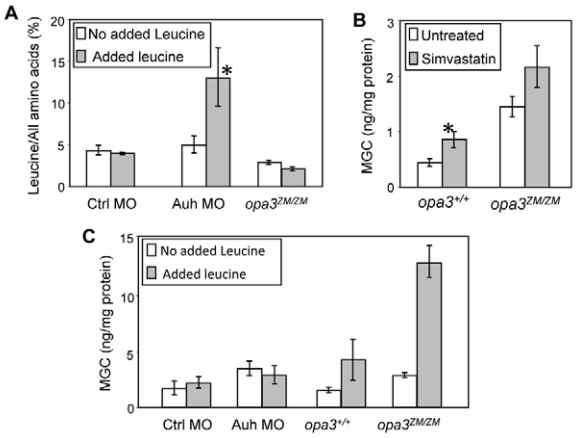

Fig. 7. *opa3*$^{ZM/ZM}$ embryos have normal leucine metabolism and their MGC production is refractory to HMG-CoA reductase inhibition. (**A**) Endogenous leucine levels in *opa3*$^{ZM/ZM}$ embryos and Auh morphants with and without leucine supplementation. Wild-type embryos injected with control MO or Auh MO, as well as uninjected *opa3*$^{ZM/ZM}$ embryos were mock treated or fed with leucine and harvested at 3 days to measure endogenous leucine levels. (**B**) MGC levels in *opa3*$^{+/+}$ and *opa3*$^{ZM/ZM}$ embryos with and without HMG-CoA reductase inhibition. Embryos were either mock treated or exposed to 0.5 μM of simvastatin at the four-cell stage and harvested at day 1 for MGC measurement. (**C**) MGC levels in *opa3*$^{ZM/ZM}$ embryos and Auh morphants with and without leucine supplementation. Wild-type embryos injected with control MO or Auh MO, as well as uninjected *opa3*$^{+/+}$ and *opa3*$^{ZM/ZM}$ embryos were mock treated or fed with leucine and harvested at 3 days to measure MGC levels. Asterisks (*) indicate statistically significant increases (*t*-test, $P<0.05$) in comparison with the controls on the left. A dramatic MGC increase was seen in leucine-supplemented *opa3*$^{ZM/ZM}$ mutants, but the significance was not quantified because only two measurements were available.

transient model for Type I MGA that we generated using antisense morpholino oligonucleotides (MOs) to block translation of the zebrafish *auh* ortholog.

Like *opa3*, maternal *auh* is expressed in four-cell embryos (see Fig. S5A in the supplementary material), then ubiquitously as embryonic *auh* until the end of gastrulation (see Fig. S5B-C in the supplementary material). Later, it becomes progressively enriched in the brain and viscera from 1-5 days of development (see Fig. S5D-F in the supplementary material). Histological sections of 3-day-old embryos reveal that *auh* is expressed in the optic nerve and the same retinal compartments as *opa3*. Injection of embryos with an Auh MO caused reductions in head and eye size, and elevated MGC levels (see Fig. S5H-J in the supplementary material).

Auh morphants displayed a substantial increase in their leucine levels in response to leucine supplementation (Fig. 7A). By contrast, leucine levels in *opa3*$^{ZM/ZM}$ embryos did not change with leucine supplementation. Thus, consistent with normal 3-hydroxyisovaleric acids levels in individuals with Costeff Syndrome, Opa3 is not required for normal leucine flux.

Based on this finding, we turned our focus to potential extra-mitochondrial sources of excess MGC in *opa3*$^{ZM/ZM}$ mutants. As described by Schroepfer (Schroepfer, 1981), MGC theoretically could be derived from extra-mitochondrial HMG-CoA by one or more mechanisms, such as the 'Popjak shunt' from dimethylallyl-pyrophosphate (PPi) first proposed by Edmond and Popjak (Edmond and Popjak, 1974) (Fig. 1B). This and other proposed pathways would require conversion of extra-mitochondrial HMG-CoA to mevalonate by HMG-CoA reductase (Fig. 1B), and so we predicted that inhibition of HMG-CoA reductase would eliminate the MGC increase in *opa3*$^{ZM/ZM}$ mutants. Treatment of zebrafish embryos with the HMG-CoA reductase inhibitor simvastatin caused a shortened body axis, which we could prevent by co-incubation with mevalonate, as reported by others (Thorpe et al., 2004). We saw no phenotypic differences between simvastatin-treated *opa3*$^{+/+}$ embryos and *opa3*$^{ZM/ZM}$ mutants (data not shown). To our surprise, we observed no reductions, but rather an increase, in the MGC levels of HMG-CoA reductase-inhibited *opa3*$^{ZM/ZM}$ mutants (Fig. 7B). We also observed an MGC increase in simvastatin-treated *opa3*$^{+/+}$ embryos, consistent with reports of MGC increases in humans undergoing statin therapy (Phillips et al., 2002).

The above data argue against excess MGC in *opa3*$^{ZM/ZM}$ mutants stemming from the leucine catabolic or mevalonate pathways. However, a third possibility was suggested by our measurements of MGC in leucine-supplemented embryos. When leucine catabolism is unimpaired, as in *opa3*$^{+/+}$ and *opa3*$^{ZM/ZM}$ embryos, leucine supplementation is predicted to cause an increase in acetyl-CoA and acetoacetate inside and outside mitochondria, with a corresponding increase in extra-mitochondrial HMG-CoA (Fig. 1B). Leucine supplementation causes an MGC increase in *opa3*$^{ZM/ZM}$, but not *opa3*$^{+/+}$ embryos (Fig. 7C). Together with our simvastatin data, this implies that OPA3 functions to facilitate metabolism of cytosolic MGC derived from extra-mitochondrial HMG-CoA through a novel, mevalonate-independent 'salvage' pathway. Unexpectedly, supplemental leucine failed to increase MGC levels in Auh morphants, suggesting the antisense knockdown was incomplete (Fig. 7C).

Sensitivity of *opa3* mutants to inhibitors of the electron transport chain

The electron transport chain (ETC) is a central component of the IMM and consists of five enzyme complexes. Considering the localization of OPA3 to the IMM, it is important to know whether OPA3 influences ETC functionality. The answer is not clear, because two individuals were reported to have ~50% reductions in ATP levels and a mouse Costeff Syndrome model was shown to have elevated levels of an ETC complex IV component (Cytochrome C Oxidase) in the optic nerve, whereas three patients were reported to have normal ETC complex activities (Anikster et al., 2001; Nissenkorn et al., 1999). We addressed this issue using an extracellular flux analyzer (Wu et al., 2007; Yao et al., 2009). We measured no differences between *opa3*$^{ZM/ZM}$ embryos and controls with regard to baseline oxygen consumption (Fig. 8A; media addition), maximal oxygen consumption (Fig. 8A; FCCP addition) or oxygen consumption after addition of ETC inhibitors (Fig. 8A; oligomycin and antimycin A additions). ATP levels were also indistinguishable between *opa3*$^{ZM/ZM}$ mutants and controls, both in their basal states and after their reduction by antimycin A treatment (Fig. 8B). Thus, loss of Opa3 does not affect ETC function per se. We also asked whether ETC disruptions affect MGC metabolism, but we observed no changes in the MGC levels of *opa3*$^{+/+}$ or *opa3*$^{ZM/ZM}$ embryos after treatment with antimycin A (see Fig. S6A in the supplementary material).

Intriguingly, despite the apparent non-involvement of Opa3 in ETC function, we see a synergistic effect of ETC inhibition and loss of Opa3 function on embryonic morphology. Each of four ETC inhibitors we tested caused variable morphological defects, which we grouped into two classes. Class I embryos have moderate developmental delays (Fig. 8C; cI), whereas class II embryos have

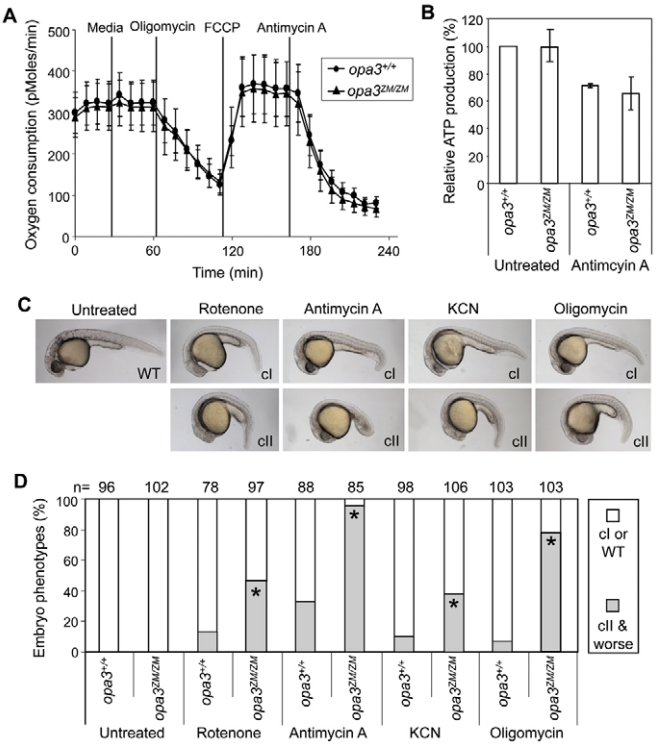

Fig. 8. Loss of Opa3 does not affect overall energy metabolism, yet sensitizes embryos to inhibitors of the electron transport chain. (**A**) Equivalent mitochondrial respiration in *opa3*$^{+/+}$ and *opa3*$^{ZM/ZM}$ embryos. Mitochondrial activity was inferred from the rate of oxygen depletion, as periodically measured in the micro-environment adjacent to groups of four 14-somite stage embryos, before and after the addition of compounds selected to maximize (FCCP) or minimize (oligomycin, antimycin A) the rate of oxidative phosphorylation. Short vertical lines indicate standard deviations and tall vertical lines show the times of each drug injection. (**B**) Equivalent ATP production in *opa3*$^{+/+}$ and *opa3*$^{ZM/ZM}$ embryos. *opa3*$^{+/+}$ embryos and *opa3*$^{ZM/ZM}$ embryos were either mock treated or treated with 1 ng/ ml antimycin A starting at the four-cell stage and harvested on day 1 for ATP measurements. (**C**) Effects of ETC inhibitors on embryonic development. Embryos were treated with four different ETC inhibitors and scored at day 1. Resulting phenotypes are shown and categorized as class I (cI) and class II (cII). (**D**) Sensitivity of *opa3*$^{ZM/ZM}$ embryos to ETC inhibitors. A substantially larger fraction of *opa3*$^{ZM/ZM}$ embryos displayed class II phenotypes after drug treatment. Asterisks (*) indicate the statistical significance of the increases (chi square test, $P<0.0001$) in comparisons with the controls on the left.

more severe delays, small heads and short or irregular tails (Fig. 8C; cII). The ETC inhibitors induced significantly more class II *opa3*$^{ZM/ZM}$ embryos than class II *opa3*$^{+/+}$ control embryos (Fig. 8D). As independent confirmation of these data, we applied antimycin A and oligomycin to embryos from heterozygous incrosses of *opa3*$^{ZM/+}$ parents, scored their phenotypes and genotyped them individually, revealing a genotype/phenotype correlation in response to each inhibitor (see Fig. S6B-C in the supplementary material). This combined disruption of Opa3 and the ETC does not affect developmental tissue specification, determined by our observation that eye-, midbrain- and tail-specific markers are robustly expressed in antimycin A-treated *opa3*$^{ZM/ZM}$ embryos (see Fig. S6D in the supplementary material).

To test whether the sensitivity of *opa3*$^{ZM/ZM}$ mutants to ETC inhibitors is specific, we assessed the effects on *opa3*$^{ZM/ZM}$ mutants and controls of two compounds that do not interact with the ETC: the HMG-CoA reductase inhibitor simvastatin and staurosporine, an apoptosis-inducing protein kinase inhibitor. As noted earlier, no differential effects were observed for simvastatin. Staurosporine sensitivity has been reported for fibroblasts from individuals with ADOAC, who carry dominant *OPA3* mutations (Reynier et al., 2004). However, we saw no difference between *opa3*$^{ZM/ZM}$ and control embryos treated with staurosporine. Thus, *opa3*$^{ZM/ZM}$ mutants are specifically sensitive to disruption of the electron transport chain.

DISCUSSION

A new animal model of Costeff Syndrome

Our ability to recapitulate Costeff Syndrome phenotypes by mutation of zebrafish *opa3* indicates that the function of this gene has been conserved through much of vertebrate evolution. *opa3*$^{ZM/ZM}$ mutants display the three defining features of Costeff Syndrome: MGC aciduria, optic nerve reduction and an extrapyramidal movement disorder (Costeff et al., 1989). The degree of MGC elevation in individuals with Costeff Syndrome is moderate, and we observe a similarly moderate elevation in *opa3*$^{ZM/ZM}$ fish. Optic nerve hypoplasia in individuals with Costeff Syndrome is detectable from infancy and often is followed by a loss of visual acuity later in life. By contrast, we detect optic nerve atrophy only in adult *opa3*$^{ZM/ZM}$ fish and find no evidence for impaired vision. The mildness of optic phenotypes in *opa3*$^{ZM/ZM}$ mutants might be due to the ability of zebrafish, but not humans, to repair optic nerve damage via regeneration (Bernhardt et al., 1996).

The recapitulation of ataxia and an extrapyramidal disorder (hypokinesia in zebrafish; bradykinesia in humans) in zebrafish *opa3*$^{ZM/ZM}$ mutants demonstrates conservation for OPA3 at the functional level and is an instructive example of how zebrafish can successfully model specific human movement disorders.

A mouse model of Costeff Syndrome caused by an *Opa3* point mutation was recently described (Davies et al., 2008). *Opa3*$^{-/-}$ mice display worse optic nerve defects than *opa3*$^{ZM/ZM}$ mutants, and a variety of movement disorders, including extrapyramidal dysfunction. The mouse phenotypes are more severe than those in individuals with Costeff Syndrome or in *opa3*$^{ZM/ZM}$ mutants, presenting with cardiac myopathy and dying by four months of age, which is less than 25% of a mouse's normal life span. By contrast, individuals with Costeff Syndrome to date enjoy normal life spans (Gunay-Aygun et al., 2010) as do *opa3*$^{ZM/ZM}$ mutants, except for the small minority with morbid swimming defects. The overall severity of the mouse model might indicate that fewer redundant or compensatory mechanisms are available to mice than to humans or zebrafish, or perhaps, as one possibility, there is a deleterious gain-of-function component to the murine *Opa3* point mutation.

No MGC measurements were made on *Opa3*$^{-/-}$ mice because of the difficulty in obtaining urine samples. We were also unable to obtain urine samples from *opa3*$^{ZM/ZM}$ mutants, so we measured MGC levels in whole embryos, which are easily generated in abundance. Indeed, the ability to obtain thousands of mutant zebrafish from a few pairs of parents enables running numerous assays on zebrafish models, as we did here. This convenience is bolstered by the ability to generate transient zebrafish disease models with antisense MOs, as shown here for Type I MGA and by others for Type II MGA (Khuchua et al., 2006).

Mitochondrial functions of OPA3

This paper provides several new insights into the functions of OPA3. First, it shows an essential requirement for OPA3 in mitochondria. Although multiple lines of evidence have pointed to a likely requirement for OPA3 in the mitochondrion, here we demonstrate that OPA3 must be delivered to mitochondria to reduce MGC levels.

Second, this paper provides evidence that OPA3 is required to maintain a normal level of MGC in the whole embryo. The precise point of action of OPA3 in MGC biosynthesis has been a long-standing enigma. Here, we confirm a previously elucidated hypothesis that OPA3 acts outside the leucine catabolic pathway, by showing that leucine catabolism is unimpaired in *opa3*$^{ZM/ZM}$ mutants (Gibson et al., 1993). Furthermore, we implicate extra-mitochondrial HMG-CoA as the proximal source of the increased level of MGC in *opa3*$^{ZM/ZM}$ mutants, suggesting that OPA3 in some manner facilitates the uptake by mitochondria of cytosolic MGC for further metabolism via the leucine catabolic pathway (Fig. 1B). The generation of MGC from cytosolic HMG-CoA might occur via steps of deacylation to free HMG followed by dehydration to MGC. Such an HMG salvage pathway is also suggested by the increased levels of MGC in human patients and in *opa3*$^{+/+}$ embryos treated with simvastatin, and an HMG salvage pathway could also account for increased MGC levels in individuals with Smith-Lemli-Opitz Syndrome, in which a distal block in cholesterol synthesis causes upregulation of HMG-CoA synthase and inhibitory actions of 7-dehydrocholesterol reduce HMG-CoA reductase activity (Kelley and Kratz, 1995; Fitzky et al., 2001; Phillips et al., 2002).

Finally, the distribution of embryonic *opa3* mRNA in the retina suggests there are regulatory mechanisms for ensuring the adequate supply of OPA3 to mitochondria. Studies have shown that mitochondrial activity in the human eye is highest in the optic nerve, the retinal ganglion cell layer, the inner and outer plexiform layers, the photoreceptor cell layer and the retinal pigment epithelium (Andrews et al., 1999). Strikingly, we observe *opa3* mRNA enrichment in the optic nerve and all but one of the retinal layers (photoreceptors) that are marked by high mitochondrial activity in humans. Based on this apparent colocalization of *opa3* mRNA and high mitochondrial activity, we suggest that the transcription and intracellular distribution of *opa3* mRNA is regulated to meet mitochondrial demand. Intriguingly, we observed the same pattern of optic nerve and retinal layer distribution for *auh* mRNA, which also encodes a mitochondrial protein (see Fig. S5 in the supplementary material). It will be of interest to learn whether other *opa3* or *auh*-mRNA-enriched tissues, such as the *opa3*-enriched intestinal epithelium, are characterized by high mitochondrial activity.

Seeking a unified etiology for OPA3 loss-of-function phenotypes

The enrichment of *opa3* mRNA in the optic nerve correlates with the occurrence of optic atrophy. Axonal localization of mRNA is uncommon, but has been reported for several other genes, particularly in immature axons (Mohr and Richter, 2000). No other anatomical defects have been reported in individuals with Costeff Syndrome, and we were unable to find any other morphogenetic abnormalities in *opa3*$^{ZM/ZM}$ mutants. Nonetheless, the expression of *opa3* in the CNS and the inner ear could be related to ataxia, its expression in the inner ear or swim bladder could be related to the buoyancy control difficulties seen in fish, and expression in the heart could be related to the cardiomyopathy in *Opa3*$^{-/-}$ mice. No digestive disorders have been observed in individuals with Costeff Syndrome or in animal models, so the medical significance of the expression of *opa3* expression in the liver and intestinal epithelium is not clear.

One of the challenges to understanding Costeff Syndrome etiology is to distinguish causes from effects. For example, the abnormal accumulation of some organic molecules has been shown to underlie optic atrophy in several diseases, raising the issue of whether elevated MGC is the cause of optic atrophy or of other neurological disorders in Costeff Syndrome (Huizing et al., 2005). Arguing against this possibility, however, is the observation that individuals with Type I MGA have much higher levels of MGC than do individuals with Costeff Syndrome but do not suffer from optic atrophy. Furthermore, artificially increased levels of MGC failed to induce hypokinesia in wild-type zebrafish larvae. Thus, elevated MGC does not appear to be the cause of optic nerve or behavioral alterations in Costeff Syndrome.

Another question is whether Costeff Syndrome symptoms result from reductions in mitochondrial energy production. This could be true for the retinal ganglion cells that form the optic nerve and certain other cells (see below). However, we see no general abnormalities of energy metabolism of zebrafish embryos that lack Opa3, and we detect no alterations in the MGC levels of zebrafish embryos whose oxidative phosphorylation has been disrupted. We conclude that OPA3 does not have a direct role in oxidative phosphorylation and that the accumulation of MGC is not caused by compromised oxidative phosphorylation. Despite this evidence for non-involvement of OPA3 in oxidative phosphorylation, we observe a potent synergy between loss of OPA3 and ETC inhibition, which supports clinical concerns of mitochondrial sensitivity in individuals with Costeff Syndrome.

Synthesizing data from this study with others, we propose that OPA3 has a role in the mitochondria that is not directly linked to oxidative phosphorylation or MGC metabolism, but rather that OPA3 serves another important role in mitochondrial energy metabolism seated in the IMM. In this model, *OPA3* loss-of-function mutations create non-deleterious, hypomorphic biochemical phenotypes in most tissues but overt phenotypes in tissues with a high local demand for mitochondrial ATP production, such as the optic nerve and neurons required for normal movement control; overt phenotypes in OPA3-deficient cells can also arise under other conditions of mitochondrial stress, such as exposure to ETC inhibitory compounds.

The principle that MGC aciduria can arise from an indirect and general mitochondrial defect has been established by Barth Syndrome/Type II MGA, which is caused by a deficiency of Tafazzin, a transacylase that regulates the fatty acyl composition and ‘maturation’ of cardiolipin (Bione et al., 1996). Cardiolipin is a major lipid in mitochondrial membranes, and Tafazzin deficiency leads to cardiolipin depletion, compromising the functional integrity of, principally, the IMM (Bione et al., 1996; Gebert et al., 2009). It is tempting to speculate that OPA3 also serves a structural role in the IMM, enabling optimal function of the electron transport chain and a subset of mitochondrial IMM proteins subserving protein and/or metabolite import.

Acknowledgements

We thank Forbes D. Porter, Christopher A. Wassif and Lien Ly for assistance with pilot studies; Kevin Bittman, Sung-Kook Hong, Huaibin Cai, Jorge L. Velez and Stephen Wincovitch for technical assistance; Charles P. Venditti and Erich Roessler for helpful discussions. This work was supported by the Intramural Research Program of the National Human Genome Research Institute, the National Institutes of Health. Deposited in PMC for release after 12 months.

Competing interests statement
The authors declare no competing financial interests.

Supplementary material
Supplementary material for this article is available at
http://dev.biologists.org/lookup/suppl/doi:10.1242/dev.043745/-/DC1

References

Andrews, R. M., Griffiths, P. G., Johnson, M. A. and Turnbull, D. M. (1999). Histochemical localisation of mitochondrial enzyme activity in human optic nerve and retina. *Br. J. Ophthalmol.* **83**, 231-235.

Anikster, Y., Kleta, R., Shaag, A., Gahl, W. A. and Elpeleg, O. (2001). Type III 3-methylglutaconic aciduria (optic atrophy plus syndrome, or Costeff optic atrophy syndrome): identification of the OPA3 gene and its founder mutation in Iraqi Jews. *Am. J. Hum. Genet.* **69**, 1218-1224.

Bernhardt, R. R., Tongiorgi, E., Anzini, P. and Schachner, M. (1996). Increased expression of specific recognition molecules by retinal ganglion cells and by optic pathway glia accompanies the successful regeneration of retinal axons in adult zebrafish. *J. Comp. Neurol.* **376**, 253-264.

Bione, S., D'Adamo, P., Maestrini, E., Gedeon, A. K., Bolhuis, P. A. and Toniolo, D. (1996). A novel X-linked gene, G4.5. is responsible for Barth syndrome. *Nat. Genet.* **12**, 385-389.

Burgess, H. A. and Granato, M. (2007). Modulation of locomotor activity in larval zebrafish during light adaptation. *J. Exp. Biol.* **210**, 2526-2539.

Costeff, H., Gadoth, N., Apter, N., Prialnic, M. and Savir, H. (1989). A familial syndrome of infantile optic atrophy, movement disorder, and spastic paraplegia. *Neurology* **39**, 595-597.

Da Cruz, S., Xenarios, I., Langridge, J., Vilbois, F., Parone, P. A. and Martinou, J. C. (2003). Proteomic analysis of the mouse liver mitochondrial inner membrane. *J. Biol. Chem.* **278**, 41566-41571.

Davies, V. J., Powell, K. A., White, K. E., Yip, W., Hogan, V., Hollins, A. J., Davies, J. R., Piechota, M., Brownstein, D. G., Moat, S. J. et al. (2008). A missense mutation in the murine Opa3 gene models human Costeff syndrome. *Brain* **131**, 368-380.

Edmond, J. and Popjak, G. (1974). Transfer of carbon atoms from mevalonate to n-fatty acids. *J. Biol. Chem.* **249**, 66-71.

Elpeleg, O. N., Costeff, H., Joseph, A., Shental, Y., Weitz, R. and Gibson, K. M. (1994). 3-Methylglutaconic aciduria in the Iraqi-Jewish 'optic atrophy plus' (Costeff) syndrome. *Dev. Med. Child Neurol.* **36**, 167-172.

Ferre, M., Bonneau, D., Milea, D., Chevrollier, A., Verny, C., Dollfus, H., Ayuso, C., Defoort, S., Vignal, C., Zanlonghi, X. et al. (2009). Molecular screening of 980 cases of suspected hereditary optic neuropathy with a report on 77 Novel OPA1 mutations. *Hum. Mutat.* **30**, E692-E705.

Fitzky, B. U., Moebius, F. F., Asaoka, H., Waage-Baudet, H., Xu, L., Xu, G., Maeda, N., Kluckman, K., Hiller, S., Yu, H. et al. (2001). 7-Dehydrocholesterol-dependent proteolysis of HMG-CoA reductase suppresses sterol biosynthesis in a mouse model of Smith-Lemli-Opitz/RSH syndrome. *J. Clin. Invest.* **108**, 905-915.

Gebert, N., Joshi, A. S., Kutik, S., Becker, T., McKenzie, M., Guan, X. L., Mooga, V. P., Stroud, D. A., Kulkarni, G., Wenk, M. R. et al. (2009). Mitochondrial cardiolipin involved in outer-membrane protein biogenesis: implications for Barth syndrome. *Curr. Biol.* **19**, 2133-2139.

Gibson, K. M., Elpeleg, O. N., Jakobs, C., Costeff, H. and Kelley, R. I. (1993). Multiple syndromes of 3-methylglutaconic aciduria. *Pediatr. Neurol.* **9**, 120-123.

Gunay-Aygun, M. (2005). 3-Methylglutaconic aciduria: a common biochemical marker in various syndromes with diverse clinical features. *Mol. Genet. Metab.* **84**, 1-3.

Gunay-Aygun, M., Gahl, W. A. and Anikster, Y. (2010). 3-Methylglutaconic Aciduria Type 3. *Gene Reviews* http://www.ncbi.nlm.nih.gov/bookshelf/br.fcgi?book=gene&part=mga3.

Ho, G., Walter, J. H. and Christodoulou, J. (2008). Costeff optic atrophy syndrome: new clinical case and novel molecular findings. *J. Inherit. Metab. Dis.* Epub ahead of print.

Huizing, M., Brooks, B. P. and Anikster, Y. (2005). Optic atrophies in metabolic disorders. *Mol. Genet. Metab.* **86**, 51-60.

Huizing, M., Dorward, H., Ly, L., Klootwijk, E., Kleta, R., Skovby, F., Pei, W., Feldman, B., Gahl, W. A. and Anikster, Y. (2010). OPA3, mutated in 3-methylglutaconic aciduria type III, encodes two transcripts targeted primarily to mitochondria. *Mol. Genet. Metab.* **100**, 149-154.

IJlst, L., Loupatty, F. J., Ruiter, J. P., Duran, M., Lehnert, W. and Wanders, R. J. (2002). 3-Methylglutaconic aciduria type I is caused by mutations in AUH. *Am. J. Hum. Genet.* **71**, 1463-1466.

Jao, L. E., Maddison, L., Chen, W. and Burgess, S. M. (2008). Using retroviruses as a mutagenesis tool to explore the zebrafish genome. *Brief. Funct. Genomic. Proteomic.* **7**, 427-443.

Kelley, R. I. and Kratz, L. (1995). 3-methylglutaconic acidemia in Smith-Lemli-Opitz syndrome. *Pediatr. Res.* **37**, 671-674.

Khuchua, Z., Yue, Z., Batts, L. and Strauss, A. W. (2006). A zebrafish model of human Barth syndrome reveals the essential role of tafazzin in cardiac development and function. *Circ. Res.* **99**, 201-208.

Kimmel, C. B., Ballard, W. W., Kimmel, S. R., Ullmann, B. and Schilling, T. F. (1995). Stages of embryonic development of the zebrafish. *Dev. Dyn.* **203**, 253-310.

Kleta, R., Skovby, F., Christensen, E., Rosenberg, T., Gahl, W. A. and Anikster, Y. (2002). 3-Methylglutaconic aciduria type III in a non-Iraqi-Jewish kindred: clinical and molecular findings. *Mol. Genet. Metab.* **76**, 201-206.

Landau, B. R. and Brunengraber, H. (1985). Shunt pathway of mevalonate metabolism. *Methods Enzymol.* **110**, 100-114.

Mohr, E. and Richter, D. (2000). Axonal mRNAs: functional significance in vertebrates and invertebrates. *J. Neurocytol.* **29**, 783-791.

Nissenkorn, A., Zeharia, A., Lev, D., Fatal-Valevski, A., Barash, V., Gutman, A., Harel, S. and Lerman-Sagie, T. (1999). Multiple presentation of mitochondrial disorders. *Arch. Dis. Child* **81**, 209-214.

Phillips, P. S., Haas, R. H., Bannykh, S., Hathaway, S., Gray, N. L., Kimura, B. J., Vladutiu, G. D. and England, J. D. (2002). Statin-associated myopathy with normal creatine kinase levels. *Ann. Intern. Med.* **137**, 581-585.

Poston, J. M. (1976). Leucine 2,3-aminomutase, an enzyme of leucine catabolism. *J. Biol. Chem.* **251**, 1859-1863.

Reynier, P., Amati-Bonneau, P., Verny, C., Olichon, A., Simard, G., Guichet, A., Bonnemains, C., Malecaze, F., Malinge, M. C., Pelletier, J. B. et al. (2004). OPA3 gene mutations responsible for autosomal dominant optic atrophy and cataract. *J. Med. Genet.* **41**, e110.

Schroepfer, G. J., Jr (1981). Sterol biosynthesis. *Annu. Rev. Biochem.* **50**, 585-621.

Sood, R., English, M. A., Jones, M., Mullikin, J., Wang, D. M., Anderson, M., Wu, D., Chandrasekharappa, S. C., Yu, J., Zhang, J. et al. (2006). Methods for reverse genetic screening in zebrafish by resequencing and TILLING. *Methods* **39**, 220-227.

Thisse, C. and Thisse, B. (1998). High Resolution Whole-Mount in situ Hybridization. In *Zebrafish Science Monitor,* Vol. 5. Eugene: University of Oregon Press.

Thorpe, J. L., Doitsidou, M., Ho, S. Y., Raz, E. and Farber, S. A. (2004). Germ cell migration in zebrafish is dependent on HMGCoA reductase activity and prenylation. *Dev. Cell* **6**, 295-302.

Wevers, R. A., de Rijk-van Andel, J. F., Brautigam, C., Geurtz, B., van den Heuvel, L. P., Steenbergen-Spanjers, G. C., Smeitink, J. A., Hoffman, G. F. and Gabreëls, F. J. (1999). A review of biochemical and molecular genetic aspects of tyrosine hydroxylase deficiency including a novel mutation (291delC). *J. Inherit. Metab. Dis.* **22**, 364–373.

Wu, M., Neilson, A., Swift, A. L., Moran, R., Tamagnine, J., Parslow, D., Armistead, S., Lemire, K., Orrell, J., Teich, J. et al. (2007). Multiparameter metabolic analysis reveals a close link between attenuated mitochondrial bioenergetic function and enhanced glycolysis dependency in human tumor cells. *Am J. Physiol. Cell Physiol.* **292**, C125-C136.

Yang, N. C., Ho, W. M., Chen, Y. H. and Hu, M. L. (2002). A convenient one-step extraction of cellular ATP using boiling water for the luciferin-luciferase assay of ATP. *Anal. Biochem.* **306**, 323-327.

Yao, J., Irwin, R. W., Zhao, L., Nilsen, J., Hamilton, R. T. and Brinton, R. D. (2009). Mitochondrial bioenergetic deficit precedes Alzheimer's pathology in female mouse model of Alzheimer's disease. *Proc. Natl. Acad. Sci. USA* **106**, 14670-14675.